Performance study of optical triangular-shaped pulse generation with full duty cycle

Ze Hao (郝 泽), Jing Li (李 晶)*, Chuangye Wang (王创业), and Jin Yuan (袁 瑾)

Key Lab of All Optical Network & Advanced Telecommunication Network of EMC, Beijing Jiaotong University, Beijing 100044, China

*Corresponding author: lijing@bjtu.edu.cn

A scheme of triangular-shaped pulses with full duty cycle generation is proposed and analyzed. Benefiting from the feature of orthogonal polarization, two approximate sinusoidal signals on different polarization states can be combined without inducing coherent interference. By tuning the time mismatching between the two signals, an approximately triangular-shaped profile can be obtained in the optical intensity. It is found that the modulation index β is no longer a fixed one, but it can be aligned within a proper range of 0.92 to 1.57. To evaluate the proposal, impacts of radio frequency voltage fluctuation, bias voltage drift, and time mismatching are discussed. Within the defined fitting error ($\eta \leq 3\%$), the tolerable range of the modulation index, time mismatching, and voltage have been found, which insures a simple operation in practice.

OCIS codes: 060.1155, 060.5625, 060.4080.
doi: 10.3788/COL201715.110601.

Photonic generation of an optical or radio frequency (RF) triangular-shaped waveform has been a topic of interest recently, which can find many applications in the all-optical converter, pulse compression, microwave photonic systems, and high-speed all-optical signal processing and manipulation[1–4]. Various approaches have been reported to generate an optical triangular-shaped waveform. One method based on optical spectrum shaping combined with frequency-to-time mapping is reported[5,6]. The drawback of the approach is the fact that they only generate triangular-shaped pulses with a small duty cycle (<1). For many applications, signals with a full duty cycle are desirable. Another alternative approach based on external modulation of a continuous-wave (CW) laser is reported to achieve high quality triangular-shaped profile. The key point is to manipulate the harmonics of optical intensity approximately equal to the first two-term Fourier components of an ideal triangular-shaped waveform. In Ref. [7], a Mach–Zehnder modulator (MZM) followed by a dispersion element is used to generate the triangular-shaped pulse. Its principle depends on the relationship between fiber dispersion and driving frequency, which leads to poor frequency tunability. In Ref. [8], spectrum manipulation of four modulation side-bands is used to generate a triangular signal with a tunable repetition rate. This scheme requires an ultra-short pulse source, which always leads to high cost and complex architecture. Then, in Ref. [9], Dai *et al.* reports a solution for versatile waveform generation (including the triangular shape) based on the optical spectral comb, which requires large signal modulation. In Ref. [10], Li *et al.* proposed a frequency-doubled triangular pulse (full duty cycle) signal generator, which requires a dual-parallel MZM driven by a sinusoidal signal. Except for the above approaches[5–10], a triangular-shaped signal can also be generated by using optical polarization manipulation[11], time domain processing[12], nonlinear polarization rotation[13], stimulated Brillouin scattering[14], and an optoelectronic oscillator[15]. In Ref. [12], a scheme of multiple waveform (including the triangular shape) generation is proposed based on time domain processing. By combining two rectangular-shaped waveforms with a specific time mismatching, triangular-shaped pulses can be generated. But this scheme is based on optical-to-electrical insensitivity of narrow-bandwidth photo-detection, which means the triangular-shaped signal can only generated in electrical domain.

In this Letter, we proposed a photonic approach to generate a triangular-shaped pulse through a single drive MZM (SD-MZM), which is driven by the RF signal. The signal from the SD-MZM is split into two paths. Benefiting from the feature of orthogonal polarization, two approximately sinusoidal signals on different polarization states can be combined without inducing coherent inference. By tuning the time mismatching between the two signals, an approximately triangular-shaped profile can be obtained in the optical intensity. Different from the approach in Ref. [12], this proposal can generate a triangular pulse in the optical domain, which will enhance its application in all-optical processing.

The schematic diagram of the proposed scheme is shown in Fig. 1. Here, the SD-MZM is biased at the quadrature point (QT). An expression of the driving sinusoidal signal is $V_{RF} \cos(\Omega t)$, where V_{RF} and Ω represent the magnitude and angular frequency of the driving RF signal; the optical field at the output of the SD-MZM can be expressed as

$$E_A(t) = E_0(t) \cos\left[\frac{\pi}{\sqrt{2}V_\pi} V_{RF}\cos(\Omega t) + \frac{\pi}{4}\right]\exp\left(j\frac{\pi}{4}\right),$$
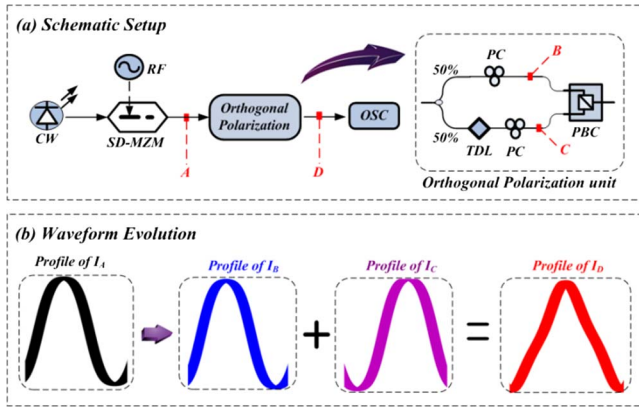
(1)

Fig. 1. (a) Schematic diagram of the optical triangular-shaped waveform construction and (b) waveform evolution diagram.

where V_π is the half-wave voltage of the SD-MZM, $E_0(t) = E_0 \exp(j\omega_0 t)$ denotes the optical field of the CW lights, in which E_0 and ω_0 are the magnitude and angular frequency. The optical intensity is given by

$$I_A \propto E_{\text{out}}(t)E_{\text{out}}^*(t) = \frac{1}{2}|E_0|^2 + \frac{1}{2}|E_0|^2 \sin[\beta \cos(\Omega t)], \tag{2}$$

where the modulation index $\beta = \sqrt{2}\,V_{\text{RF}}/V_\pi$ is dependent on V_{RF}, the magnitude of the driving signal.

Figure 2 illustrates the transmission of the SD-MZM and a diagram of profile mapping. From Fig. 2, the profile of RF signal can be mapped to optical intensity when the SD-MZM is biased at the QT. To obtain approximate sinusoidal intensity profiles, the magnitude $\sqrt{2}\,V_{\text{RF}}$ should be not more than $V_\pi/2$. As has been expressed above, the upper limit of modulation can be obtained as $\beta \leq 1.57$.

Then, an orthogonal polarization unit is utilized to construct the waveform. As shown in Fig. 1(a), it consists of two polarization controllers (PCs), a tunable time delay line (TDL), and a polarization beaming combiner (PBC).
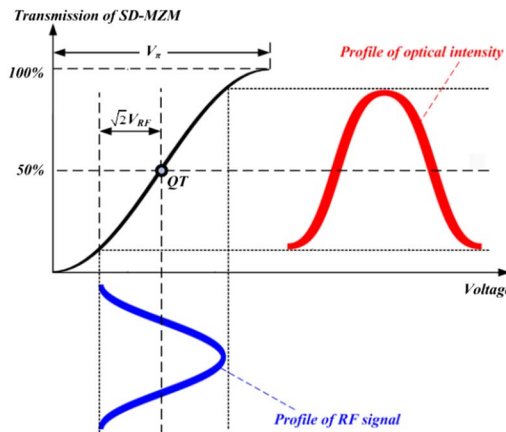

Fig. 2. Transmission of the SD-MZM and diagram of profile mapping from the RF signal to optical intensity.

The signal from the SD-MZM is split into two paths. The upper- and lower-path light-waves are then aligned with orthogonal polarization direction via a PC. In order to introduce a time mismatching τ between two paths, a tunable TDL is connected to the lower path. After that, a PBC is used to combine the signals. The optical field can be written as

$$E_D(t) = \left\{ \hat{x} \frac{E_0(t)}{\sqrt{2}} \cos\left[\frac{\pi}{\sqrt{2}V_\pi} V_{\text{RF}} \cos(\Omega t) + \frac{\pi}{4} \right] \exp\left(j\frac{\pi}{4}\right) \right.$$
$$+ \hat{y} \frac{E_0(t-\tau)}{\sqrt{2}} \cos\left\{ \frac{\pi}{\sqrt{2}V_\pi} V_{\text{RF}} \cos[\Omega(t-\tau)] + \frac{\pi}{4} \right\}$$
$$\left. \times \exp\left(j\frac{\pi}{4}\right) \right\}. \tag{3}$$

Since the signals in upper and lower paths are combined with orthogonal polarization, there will be no coherence interference between them. Thus, the corresponding optical intensity of I_D can be expressed as

$$I_D \propto E_D(t)E_D^*(t) = \underbrace{\frac{|E_0|^2}{4} + \frac{|E_0|^2}{4}\sin[\beta\cos(\Omega t)]}_{I_B}$$
$$+ \underbrace{\frac{|E_0|^2}{4} + \frac{|E_0|^2}{4}\sin\{\beta\cos[\Omega(t-\tau)]\}}_{I_C} \tag{4}$$

Note that the output optical intensity is the combination of $I_B(t)$ and $I_C(t)$. The waveform evolution can be found in Fig. 1(b). In order to find the relationship between the triangular-shaped profile and the parameters in this prototype (i.e., β, τ, and Ω), Eq. (4) is expanded by the Jacobi–Anger expansion as follows:

$$I_D \propto dc - \sum_{n=1}^{\infty}(-1)^n J_{2n-1}(\beta)\cos\left[\frac{(2n-1)}{2}\Omega\tau\right]$$
$$\times \cos\left[(2n-1)\Omega\left(t+\frac{\tau}{2}\right)\right]$$
$$= dc - A_1\cos\left[\Omega\left(t+\frac{\tau}{2}\right)\right] - A_3\cos\left[3\Omega\left(t+\frac{\tau}{2}\right)\right] - o(\Omega), \tag{5}$$

where $\begin{cases} A_1 = -2J_1(\beta)\cos\left(\frac{\Omega\tau}{2}\right) \\ A_3 = 2J_3(\beta)\cos\left(\frac{3\Omega\tau}{2}\right) \end{cases}$ and $o(\Omega)$ represents high-order harmonics, which can be neglected when modulation index β is small. The Fourier expansion of an ideal triangular-shaped waveform is given by

$$T(t) = dc - \cos\omega t - \frac{1}{9}\cos 3\omega t - \cdots$$
$$- \frac{1}{(2k-1)^2}\cos[(2k-1)\omega t]. \tag{6}$$

To obtain an optical triangular-shaped pulse that is close to an ideal triangular shape, an approximation

should be made between I_D and $T(t)$. Thus, the following relationship should be satisfied:

$$A_1 = 9A_3. \tag{7}$$

Substituting A_1 and A_2 into Eq. (7) and solving the equation, we can obtain the relationship between β and $\Omega\tau$ as

$$4\cos^2\left(\frac{\Omega\tau}{2}\right) = \frac{27J_3(\beta) - J_1(\beta)}{9J_3(\beta)}. \tag{8}$$

For a given $\Omega\tau$, β can always be figured out by solving Eq. (8). In order to make this equation solvable, the relationship of $27J_3(\beta) - J_1(\beta) \geq 0$ should be satisfied first. After calculation, we can get the lower limit of the modulation index as $\beta \geq 0.92$. In the above analysis, we already have the upper limit of the modulation index as $\beta \leq 1.57$. Therefore, the whole tuning range of β is found as $0.92 \leq \beta \leq 1.57$.

By solving Eq. (8), we may have multiple solutions of $\Omega\tau$. In order to simplify the calculation, we only consider the first periodic solutions, $0 \leq \Omega\tau \leq 2\pi$, taking the driving RF $f_{\mathrm{RF}} = 10, 12$, and 14 GHz, for example. Figure 3 plots the desired time mismatching τ at different β. From Fig. 3, for a given f_{RF}, a fixed β is not required anymore. In this scheme, β can be chosen randomly within the range of 0.92 to 1.57. Then, by simply tuning τ, Eq. (8) can be satisfied, which means $T(t)$ in Eq. (6) can be simply expressed by I_D in Eq. (5). An approximately triangular-shaped pulse can be obtained in the optical intensity. Besides, as shown in the figure, f_{RF} is different when τ is changed, which means the frequency tunability can be implemented by merely adjusting τ.

To validate the theory, simulations are performed according to the schematic setup, as shown in Fig. 1. An optical signal from a CW laser with a central wavelength of 1550 nm and a line-width of 10 MHz is sent to an SD-MZM. The SD-MZM possesses an insertion loss of 5 dB, half-wave switching voltage of 4 V, bias voltage
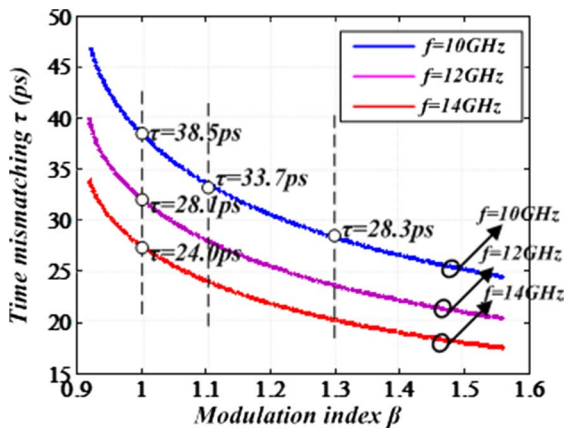
difference of 2 V, and extinction ratio of 20 dB. The SD-MZM is biased at the QT. The modulation index β can be chosen randomly from 0.92 to 1.57, which can be achieved by changing the magnitude of the RF signal.

Figure 4 shows the simulation results for the generation of a 10 GHz triangular-shaped pulse. The normalized optical intensity profile of I_B, I_C, and I_D, are shown in this figure. Here, the modulation index and time mismatching are set to $\beta = 1.1$ and $\tau = 33.7$ ps, according to the prediction in Fig. 3. The evolution of the optical intensity profiles can be observed in these figures.

In order to evaluate the generated waveform more efficiently, the parameter of fitting error η is defined as

$$\eta = \sqrt{\frac{\sum_{k=1}^{m}(X_k - Y_k)^2}{\sum_{k=1}^{m}(X_k^2 + Y_k^2)}} \times 100\%, \tag{9}$$

where m is the number of the sampling points in a period, X_k is the kth sampled amplitude of the target waveform (I_D in our case), and Y_k is the kth sampled amplitude of the search waveform [$T(t)$ in Eq. (6)]. Therefore, the fitting error η can simply be used to judge the similarity of the generated waveform. Normally, when the fitting error is small enough (i.e., less than 3%), the generated pulse can be considered desirable. In theory, when η equals zero, the target waveform can be regarded as the optimum waveform. However, this goal cannot be achieved in practice. What we can do is make sure that η is as small as possible.

We find that the modulation index can be chosen within a suitable range rather than a fixed one. But, when the time mismatching and bias voltage are set, the most suitable modulation index β is determined accordingly. For example, in Fig. 3, when the frequency is $f_{\mathrm{RF}} = 10$ GHz, and the time mismatching is $\tau = 33.7$ ps, the

Fig. 3. (Color online) Relationship between the desired time mismatching τ and modulation index β at different driving frequency $f_{\mathrm{RF}} = 10, 12$, and 14 GHz.
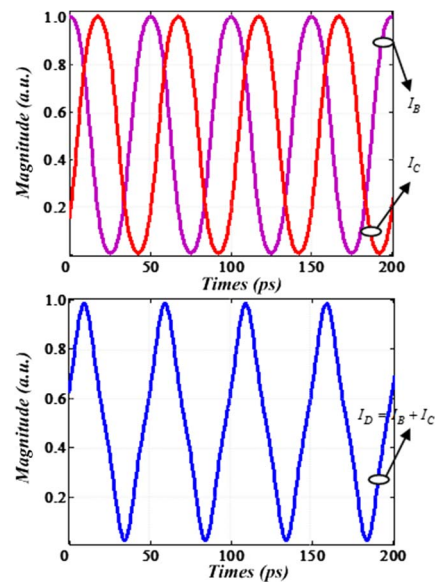

Fig. 4. (Color online) Simulation intensity profile of I_B, I_C, and I_D.

optimum β is 1.1. In theory, the modulation index is set to 1.1 with no drift. However, any voltage fluctuation of the RF signal will slightly change the desired modulation index. Here, we will mainly discuss the impact of modulation index drifts. To do that, we focus on fitting error evolution at a different β. Figure 5 shows the variation curve of the fitting error when the modulation index increases from 0.9 to 1.35. As shown in Fig. 5, when β equals 1.1, the value of the η is 2.6%, which is very close to zero. In other words, the generated waveform can be considered a triangle.

Within the defined fitting error of $\eta \leq 3\%$, the tolerate range of modulation index β is found as $0.99 \leq \beta \leq 1.16$, corresponding to -10% to 5% drift of the optimum value ($\beta = 1.1$). For another parameter setting (i.e., f_{RF} and τ), the optimum β may change. But, the acceptable drift range can still be found.

When the bias state of the SD-MZM is adjusted to a precise QT, the undesired harmonic (i.e., second and fourth) in Eq. (5) can be well suppressed. However, in practice, the bias drift problem (or bias voltage jitter) always exists and will surely degrade the similarity of the output waveform. Therefore, we will discuss this issue in this part. Here, the half-wave switching voltage V_π is 4 V, and the optimum bias voltage is 2 V. In order to analyze the influence of the bias drift, we will focus on the fitting error and harmonic distortion suppression ratio (HDSR). The HDSR is defined as the power ratio of the first-order harmonic and the undesired second-order harmonic. Normally, the value of the HDSR can simply indicate the impact of the undesired harmonic in I_D. For example, when the HDSR is higher than 40 dB, the second-order harmonic can be considered fully suppressed, and its impact to the final waveform is negligible. Figure 6 shows the relationship between the bias voltage and fitting error. As shown in Fig. 6, at the optimum bias state $V_{\mathrm{bias}} = 2\,\mathrm{V}$, the fitting error reaches the minimum value at 2.6%. When the bias voltage range is 1.94 to 2.06 V, it corresponds to a -3% to 3% drift from the optimum voltage. The fitting error $\eta \leq 3\%$ and the obtained waveform is appropriate. However, when the bias voltage changes beyond the range, the fitting error greatly
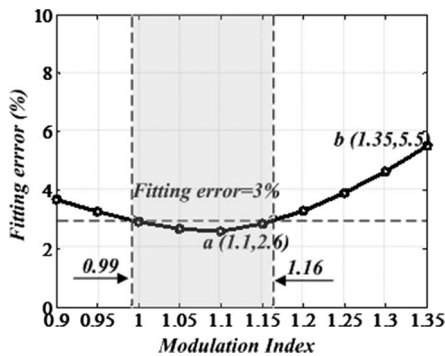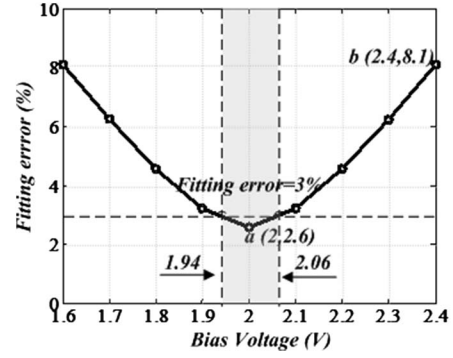

Fig. 6. Variation curve of the fitting error when the bias voltage changes from 1.6 to 2.4 V.

increases, which will not fit for generating a triangular-shaped pulse.

According to the above discussion, the bias drift problem of the SD-MZM will introduce the undesired second-order harmonic. The greater the range of drift, the worse the waveform changes. In order to minimize this impact, the bias voltage drift should be controlled in the range of -3% to 3%, which can be realized by using the bias voltage circuit.

From the previous discussion we know that when the modulation index $\beta = 1.1$, and the bias voltage $V_{\mathrm{bias}} = 2\,\mathrm{V}$ are determined, the triangular-shaped pulse of the desired frequency can be obtained by adjusting the time mismatching τ. When the time mismatching is set as the optimum value of $\tau = 33.7$ ps, we can obtain a triangular-shaped pulse. However, in practice, it is difficult to adjust the time mismatching to an exact value. The time mismatching jitter is mainly induced by the tuning accuracy of the TDL. In order to analyze this impact, the relationship between the time mismatching and fitting error is shown in Fig. 7. Note that at the optimum of $\tau = 33.7$ ps, the fitting error is a minimum of $\eta = 2.6\%$. The resulting waveform can be predicted as a triangle. When τ is controlled within 31 to 39 ps, the fitting error is less than 3%. Therefore, an approximately triangular pulse can still be obtained. However, when τ is continuously changing, the fitting error will exceed the boundary, and the output waveform will not be a triangle any more.

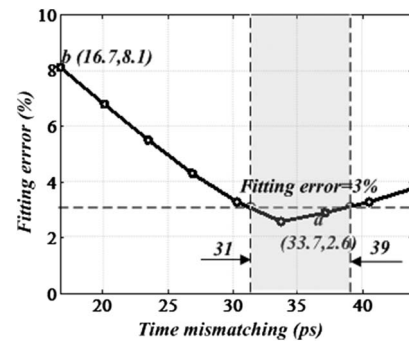Fig. 5. Variation curve of the fitting error when the modulation index changes from 0.9 to 1.35.

Fig. 7. Variation curve of the fitting error when the time mismatching changes from 16.7 to 43.9 ps.
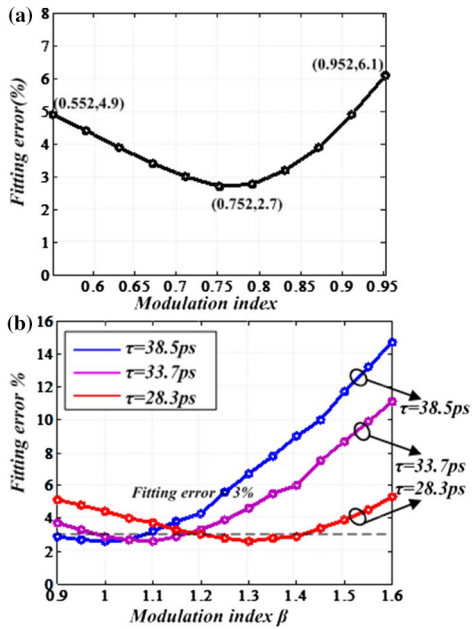
Fig. 8. (Color online) (a) Relation curve between the fitting error and the modulation coefficient in Ref. [12]. (b) The relation curve between the fitting error and the modulation index with $\tau = 38.5$, 33.7, and 28.3 ps in this scheme.

In general, the time mismatching should be adjusted in the range of 31 to 39 ps, corresponding to -14% and 16% drift from the optimum value. Of course, if the time mismatching is closer to 33.7 ps, the better the resulting waveform.

To figure out the differences between our scheme and the work in Ref. [12], we conduct the scheme in Ref. [12] and our proposal under the same simulation environment. First, we validate the simulation using the parameters in Ref. [12]. In theory, the principles of the two schemes are identical, by combining two similar waveforms to construct a triangle. The major difference is that a fixed modulation index is not required in this model. Figure 8(a) shows the simulated fitting error versus the modulation index in Ref. [12]. Note that the optimum modulation index is 0.752, which agrees with the research in Ref. [12]. It can be found that the minimum fitting error is 2.7%, and the curve is similar to the result of Fig. 5. The slight difference may be induced by the different β. A good agreement with the experiment is predicted. In Ref. [12], the modulation index should be fixed at 0.752, which is not convenient in practice. In this scheme, the modulation index is not fixed anymore. When the modulation index is between 0.92 and 1.57, the eligible time mismatching can always be found. Figure 8(b) shows the curves of different modulation indexes when the time mismatchings are

$\tau = 28.3$, 33.7, and 38.5 ps. When the modulation index is set, the desired triangular waveform can be obtained by adjusting the time mismatching, which makes the operation simple in practice. Besides, our proposal can generate triangular pulses in the optical domain, which will enhance its application in all-optical processing.

In conclusion, an optical triangular-shaped pulse with a full duty cycle generation approach is proposed. To evaluate the performance, a fitting error η is defined to judge the similarity of the generated pulse. The parameters discussed are used, and some useful results are obtained. For example, the modulation index deviates from the optimum value of -10% to 5%, and the ideal triangular pulse can still be obtained. The bias voltage should be controlled between -3% and 3% of the optimum value. In order to get the ideal triangular pulse, the time mismatching should be adjusted to the range of -14% and 16% drift from the optimum value. These discussions make the scheme more practical.

References
1. R. S. Bhamber, A. I. Latkin, S. Boscolo, and S. K. Turitsyn, in *34th European Conference on Optical Communication (ECOC 2008)* (2008), paper Th.1.B.2.
2. A. I. Latkin, S. Boscolo, R. S. Bhamber, and S. K. Turitsyn, J. Opt. Soc. Am. B **26**, 1492 (2009).
3. J. Li, T. Ning, L. Pei, J. Zheng, J. Sun, Y. Li, and J. Yuan, Chin. Opt. Lett. **13**, 080606 (2015).
4. Z. He, W. Liu, B. Shen, X. Chen, X. Gao, S. Shi, Q. Zhang, D. Shang, Y. Ji, and Y. Liu, Chin. Opt. Lett. **14**, 040602 (2016).
5. S. Boscolo, A. I. Latkin, and S. K. Turitsyn, IEEE J. Quantum Electron. **44**, 1196 (2008).
6. J. Ye, L. Yan, W. Pan, B. Luo, X. Zou, A. Yi, and S. Yao, Opt. Lett. **36**, 1458 (2011).
7. J. Li, X. Zhang, B. Hraimel, and T. Ning, J. Lightwave Technol. **30**, 1617 (2012).
8. J. Li, T. Ning, L. Pei, and W. Jian, IEEE Photon. Technol. Lett. **25**, 952 (2013).
9. B. Dai, Z. Gao, X. Wang, and H. Chen, J. Lightwave Technol. **31**, 145 (2013).
10. J. Li, Z. Hao, L. Pei, T. Ning, and J. Zheng, Chin. Opt. Lett. **15**, 090603 (2017).
11. C. Ma, Y. Yiang, G. Bai, Y. Tang, X. Qi, Z. Jia, Y. Zi, and J. Yu, Opt. Commun. **363**, 207 (2016).
12. Y. Jiang, C. Ma, G. Bai, and Z. Ji, Opt. Express **23**, 19442 (2015).
13. W. Li, W. Wang, W. Sun, W. Wang, J. Liu, and N. Zhu, Opt. Lett. **39**, 4758 (2014).
14. X. Liu, W. Pan, X. Zou, D. Zheng, L. Yan, B. Luo, and B. Lu, J. Lightwave Technol. **32**, 3797 (2014).
15. W. Wang, W. Li, W. Sun, and W. Wang, IEEE Photon. Technol. Lett. **27**, 522 (2015).